open-circuit voltage and fill factor, are comparable. This further suggests that nanorod length not diameter determines device performance. Moreover, band gap tuning in nanorods enables the realization of high-efficiency device architectures, such as tandem solar cells in which the different band gaps can be obtained by modifying only one chemical compound.

We can understand the origin of the high efficiency of nanorod-polymer devices by studying the dependence of charge transport on nanorod length. The external quantum efficiency (EQE), which is the percentage of electrons collected per incident photon (with no correction for reflection losses), can be used as a measure of the efficiency of charge transport given that the following quantities are comparable for a set of devices: (i) incident light intensity; (ii) fraction of light absorbed; (iii) charge collection efficiency at the electrodes, which is mainly given by the choice of electrodes; and (iv) the charge transfer efficiency, as determined from photoluminescence quenching. These four conditions are met for the devices for which EQE data are presented in Fig. 4A. Therefore, we can conclude that as the aspect ratio of the nanorods increases from 1 to 10, the charge transport must improve substantially to yield an EQE enhancement by a factor of approximately 3. In networks consisting of shorter nanoparticles, electron transport is dominated by hopping and, in those consisting of longer particles, band conduction is prevalent. In a cross section of the blend film (Fig. 3D), most nanorods were oriented partly in the direction of the electric field and, thus, in the direction of electron transport. Because the thickness of the nanorod-polymer film is ~200 nm, 60-nm-long nanorods can penetrate through a large portion of the device whereas 30-nm and 7-nm-long particles are progressively less effective (Fig. 3C). The best device, which contained 7 nm by 60 nm nanorods, performed with a maximum EQE of 55% under 0.1 mW/cm^2 illumination at 485 nm (Fig. 4A), and this value has been remarkably reproducible (*20*).

In order for plastic nanorod devices to achieve typical power conversion efficiencies of conventional inorganic solar cells, it is necessary to reduce charge recombination, which decreases the EQE and the FF at solar light intensities. An increase in carrier mobilities would realize this by decreasing the carrier concentration within the device. Further enhancement of carrier mobilities can be accomplished by improving the nanocrystal-polymer interface to remove nanorod surface traps, aligning the nanorods perpendicular to the substrate, and further increasing their length.

References and Notes

1. S. E. Shaheen *et al.*, *Appl. Phys. Lett.* **78**, 841 (2001).
2. M. A. Green, K. Emery, D. L. King, S. Igari, W. Warta, *Prog. Photovoltaics* **9**, 287 (2001).
3. L. Bozano, S. A. Carter, J. C. Scott, G. G. Malliaras, P. J. Brock, *Appl. Phys. Lett.* **74**, 1132 (1999).
4. G. Yu, J. Gao, J. C. Hummelen, F. Wudl, A. J. Heeger, *Science* **270**, 1789 (1995).
5. L. S. Roman, M. R. Andersson, T. Yohannes, O. Inganas, *Adv. Mater.* **9**, 1164 (1997).
6. J. J. Dittmer, E. A. Marseglia, R. H. Friend, *Adv. Mater.* **12**, 1270 (2000).
7. H. Bässler, *Molec. Crys. Liq. Crys. Sci. Technol. Sec. A* **252**, 11 (1994).
8. N. C. Greenham, X. G. Peng, A. P. Alivisatos, *Phys. Rev. B* **54**, 17628 (1996).
9. D. S. Ginger, N. C. Greenham, *Phys. Rev. B* **59**, 10622 (1999).
10. J. M. Rehm *et al.*, *J. Phys. Chem.* **100**, 9577 (1996).
11. A. P. Alivisatos, *Science* **271**, 933 (1996).
12. X. G. Peng *et al.*, *Nature* **404**, 59 (2000).
13. Z. A. Peng, X. G. Peng, *J. Am. Chem. Soc.* **123**, 183 (2001).
14. H. Sirringhaus, N. Tessler, R. H. Friend, *Science* **280**, 1741 (1998).
15. W. U. Huynh, X. G. Peng, A. P. Alivisatos, *Adv. Mater.* **11**, 923 (1999).
16. We used between 5 and 15% pyridine in chloroform. The optimal amount of pyridine is determined by the number of nonpassivated Cd surface sites on the nanorods. An excess of pyridine, however, is to be avoided, as this mediates the precipitation of P3HT, which is insoluble in pyridine. Replacing chloroform with this solvent mixture leads to an increase in energy conversion efficiency of more than 50%.
17. The FF is defined as FF $= \frac{\{I \cdot V\}_{max}}{I_{SC} \cdot V_{OC}}$ where I_{SC} and V_{OC} are short circuit current and open circuit voltage, respectively. The power conversion efficiency is $\eta = \frac{FF \cdot I_{SC} \cdot V_{OC}}{\text{light intensity}}$. The power conversion efficiency can be calculated both under monochromatic and white light (such as solar) illumination.
18. The sun simulator essentially consists of a 75 W xenon source and a set of Oriel A.M. 0 and A.M. 1.5 filters (Stratford, CT). The temperature was maintained at 25°C, verified by an in situ thermocouple by flowing argon past the device during measurements. The spectral overlap and intensity integral between the A.M. 1.5 Global standard (with spectral standard, ASTM E892 Global, and intensity of 96.4 mW/cm^2) and our sun simulator were optimized for the wavelength region in which the active layer shows absorption. The error in the simulation with regards to the obtained photocurrent is ~10%.
19. B. O'Regan, M. Grätzel, *Nature* **353**, 737 (1991).
20. The results reported represent the median of five sets of devices made on separate occasions from three different synthetic batches of CdSe totaling 57 individual solar cells. The maximum external quantum efficiency of each of these 57 devices are all within 10% relative to the median with the highest obtained efficiency at 59%, all under ~0.1 mW/cm^2 monochromatic illumination. Individual devices have been characterized repeatedly over the time scale of several months and showed no substantial change between measurements.

21. Supported by the National Renewable Energy Laboratory (grant XAD-9-18668-02) and the DOE (contracts DE-AC03-76SF00098 and DE-AC03-76SF00098). We are grateful to the Robert D. Ogg Electron Microscopy Laboratory at the University of California, Berkeley, for assistance with the TEM work and providing cross sections. The authors also would like to thank G. Whiting and W. Libby for experimental assistance and L. Manna, D. Milliron, J. Frechet, and C. Pitois for their valuable discussions. W.U.H. thanks the Natural Sciences and Engineering Research Council of Canada for a fellowship.

19 December 2001; accepted 19 February 2002

Theory of Quantum Annealing of an Ising Spin Glass

Giuseppe E. Santoro,[1] Roman Martoňák,[2,3] Erio Tosatti,[1,4]* Roberto Car[5]

Probing the lowest energy configuration of a complex system by quantum annealing was recently found to be more effective than its classical, thermal counterpart. By comparing classical and quantum Monte Carlo annealing protocols on the two-dimensional random Ising model (a prototype spin glass), we confirm the superiority of quantum annealing relative to classical annealing. We also propose a theory of quantum annealing based on a cascade of Landau-Zener tunneling events. For both classical and quantum annealing, the residual energy after annealing is inversely proportional to a power of the logarithm of the annealing time, but the quantum case has a larger power that makes it faster.

The annealing of disordered and complex systems toward their optimal (or lowest energy) state is a central problem in statistical physics. The unknown ground state of a system can be approximated by slow-rate cooling of a real or fictitious temperature: The slower the cooling, the closer the approximation gets to the optimal solution (*1, 2*). Although this kind of standard classical annealing (CA) has been extensively investigated over the last two decades (*1–3*) and is routinely used in a variety of technological applications, such as chip circuitry design, any improved optimization algorithm would certainly be of enormous value.

Recent results on the spin ½ disordered Ising ferromagnet $LiHo_{0.44}Y_{0.56}F_4$ (*4, 5*) suggested that quantum annealing (QA) works better than CA. In QA, temperature is replaced by a quantum mechanical kinetic term; in the specific case, this term is a transverse magnetic field, Γ, mixing the up and down spin states at each site. Initially the quantum perturbation starts out so large in magnitude as to completely disorder the system even at zero temperature. When the transverse field is subsequently re-

duced to zero at some slow rate $1/\tau$, the system is "annealed" toward its ground state, much in the same way as when its temperature is reduced to zero in CA. The question is which of the two, CA or QA, works better, and how and why. Experimental comparison (*4*) of the properties displayed by the same system transported through two different routes in the $[T, \Gamma]$ plane from the same initial state A (a classical high-T state) to the same nominal final state B (a low-T glassy state) indicates that QA, the "quantum route" from A to B, yields (with the same "cooling" rate) a state B apparently closer to the ground state than that yielded by CA, the classical route. The data, however, do not clarify why that should be so.

Theoretical suggestions and exemplifications of QA made by various groups over the past decade (*6–10*) have stimulated considerable interest in understanding the mechanism of QA better. A theoretical discussion of the relative merits of CA and QA is therefore desirable. For this, it is necessary to carry out a direct comparative test on a sufficiently representative benchmark system, such as a spin glass, and to lay the bases of a theory of the processes underlying QA. Even in the context of CA, open issues remain. For instance, the way the final annealed energy $E_{\mathrm{final}}(\tau)$ approaches the ground-state energy E_{GS} as a function of the annealing rate $1/\tau$ is still controversial. Whereas general theoretical arguments by Huse and Fisher (*3*) predict a slow logarithmic decrease of the residual energy $\varepsilon_{\mathrm{res}}(\tau) = E_{\mathrm{final}}(\tau) - E_{\mathrm{GS}} \approx \log^{-\zeta}(\tau)$, with $\zeta \leq 2$, early simulations (*11*) and more recent studies (*12, 13*) favor a different form such as power-law, $\varepsilon_{\mathrm{res}}(\tau) \approx \tau^{-\alpha}$, or stretched exponential. The question remains whether the discrepancy between simulations and theory is real, or only apparent.

At the outset, inspired by Brooke *et al.*'s experimental system (*4, 5*), we selected the two-dimensional (2D) random Ising model as an appropriate realistic test case. This choice is dictated by the fact the 2D random Ising model is technically a polynomial problem (*14*)—where E_{GS} can be calculated up to sufficiently large lattice sizes (*15*) [thus avoiding an extra fitting parameter in $\varepsilon_{\mathrm{res}}(\tau)$]—which is nonetheless of prohibitively large complexity for any physical dynamics as a true glass (*3, 16*). On this system we carried out CA and QA, and found that QA is indeed faster. For CA we find that $\varepsilon_{\mathrm{res}}(\tau)$ deviates from a power law at large τ and is compatible with the Huse-Fisher law $\varepsilon_{\mathrm{res}}(\tau) \approx \log^{-\zeta}(\tau)$. We then built a theory of QA of a spin glass based on the idea of a cascade of level crossings. Our theory suggests an asymptotic decay $\varepsilon_{\mathrm{res}}(\tau) \approx \log^{-\zeta_{\mathrm{QA}}}(\tau)$ that is again logarithmic, as in CA, but is governed by somewhat different exponents that make it faster.

The Edwards-Anderson Hamiltonian of an Ising spin glass in transverse field is

$$H = -\sum_{\langle ij \rangle} J_{ij}\sigma_i^z\sigma_j^z - \Gamma\sum_i \sigma_i^x \qquad (1)$$

where nearest-neighbor spins $\langle ij \rangle$ of a cubic lattice in D dimensions interact with a random exchange coupling J_{ij}, Γ is the transverse field inducing transitions between the two states, $\uparrow$ and $\downarrow$, of each spin, and σ_i^x, σ_i^z are Pauli matrices at site i. The problem is to anneal this system as closely as possible to its classical ($\Gamma = 0$) ground state. In CA (*1, 2*), there is no quantum mechanics ($\Gamma = 0$): One starts with a sufficiently high temperature T_0, which is then reduced linearly to zero in a time τ. In QA, T is instead fixed to zero or some small value, and one starts with a transverse field Γ_0 sufficiently large to throw the system into a disordered quantum paramagnetic state, decreasing Γ linearly to zero, again in a time τ.

Because real-time annealing is computationally out of the question for the large systems addressed here, we work with the fictitious "time" represented by the number of Monte Carlo (MC) steps. For our implementation of CA, we used a standard Metropolis MC; for QA we used a path integral MC (PIMC) (*17, 18*) scheme for a quantum system at a small finite temperature T. The 2D quantum Ising model is first mapped on a (2 + 1)D classical model consisting of P copies (Trotter replicas) of the original lattice, with a nearest-neighbor uniform ferromagnetic coupling in the third (Trotter) direction $J^{\perp} = -(PT/2)\log\tanh(\Gamma/PT)$, at temperature PT (*17, 18*). When Γ is large, the replicas are only weakly coupled. As Γ decreases to zero, $J^{\perp}$ increases, eventually forcing all replicas into the same configuration. For a given 2D lattice size $L \times L$ (L up to 80) and for a fixed realization of the J_{ij}, drawn from a flat distribution in the interval $(-2, 2)$, we got the exact classical E_{GS} (*15*) and then carried out repeated annealings (45 for $L = 80$), both CA and QA. The annealing parameters T (for CA) or Γ (for QA) were decreased stepwise from the initial value of $T_0 = 3$ or $\Gamma_0 = 2.5$ down to zero, with a total of τ MC steps per spin (*18*).

The residual energy $\varepsilon_{\mathrm{res}}(\tau)$ for $L = 80$ is plotted in Fig. 1 against τ, actually the MC computer time, for both CA and QA. QA appears definitely superior to CA, with a lower $\varepsilon_{\mathrm{res}}(\tau)$ for large τ. This theoretical finding is consistent with the experimental evidence of significantly faster relaxation times observed in QA (*4*). The τ dependence of our QA data does depend on the chosen values of P and T, particularly on the value of PT, whose optimal value appears to be around $PT = 1$. An increase of P for a fixed value of PT (Fig. 1, inset) ceases to be effective beyond a certain characteristic length (depending on PT) in the Trotter direction. The computational cost increases linearly with P, and the choice $P = 20$ (corresponding to $T = 0.05$) was found to be optimal up to the largest values of τ used.

A feature evident in our $\varepsilon_{\mathrm{res}}(\tau)$ CA data is the small but consistent deviation from a pure power law, suggesting serious reconsideration of all the earlier power-law claims (*11, 12*). Because the slope (or apparent power) systematically declines for increasing τ, it is natural to ask whether it will asymptotically extrapolate to zero in accordance with the Huse-Fisher logarithmic law (*3*). If we write this law in the form $\varepsilon_{\mathrm{res}}{}^{-1/\zeta} = A\log(\gamma\tau)$, where A is a prefactor and

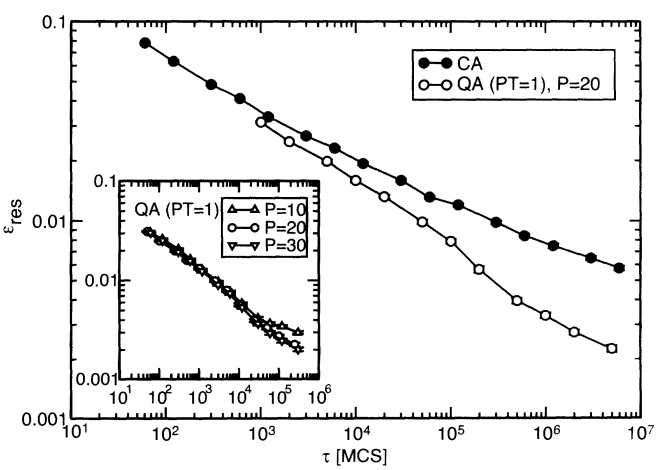

Fig. 1. Comparison of the residual energy per site for an 80 × 80 disordered 2D Ising model after classical and quantum annealing. The QA data shown correspond to the optimal value of $PT = 1$, with $T = 0.05$ and $P = 20$ Trotter replicas. For fair comparison, the annealing time τ used in the QA has been rescaled (multiplied by P) so that points at the same τ require the same computer time (MCS, Monte Carlo steps). The lower residual energy signifies that QA is superior to CA. Inset: τ-unrescaled QA data for the same system for increasing values of P. Note the satisfactory convergence for $P = 20$.

[1]Scuola Internazionale Superiore di Studi Avanzati (SISSA) and Istituto Nazionale per la Fisica della Materia (INFM) (Unità di Ricerca SISSA), I-34014 Trieste, Italy. [2]Swiss Centre for Scientific Computing, CH-6928 Manno, Switzerland, and Department of Physical Chemistry, ETH-Zürich, CH-8093 Zürich, Switzerland. [3]Department of Physics, Slovak Technical University (FEI), 81219 Bratislava, Slovakia. [4]International Center for Theoretical Physics (ICTP), Post Office Box 586, I-34100 Trieste, Italy. [5]Department of Chemistry and Princeton Materials Institute, Princeton University, Princeton, NJ 08544, USA.

*To whom correspondence should be addressed. E-mail: tosatti@sissa.it

γ is a rate constant, and replace the time with the number of MC steps, we can plot the CA data as in Fig. 2. The extrapolated behavior is indeed compatible with a straight line. However, as Fig. 2 shows, it is impossible to extract a value for the exponent ζ; in particular, we cannot establish whether $\zeta \leq 2$ (*3*) is any better, as might have been expected.

To shed some light on the actual asymptotic form of residual energy in QA, we begin with a cartoon of the instantaneous energy spectrum of Eq. 1 versus Γ (Fig. 3), suggested by small-systems exact diagonalizations. For sufficiently large initial $\Gamma_0 \gg |J_{ij}|$, the ground state, generally nondegenerate (*19*), must have a finite excitation gap. Imagine following the Schrödinger evolution of an initial ground-state wave function $|\Psi_{\Gamma_0}(t = 0)\rangle$ while reducing Γ gradually to zero as a function of time (*10*). The instantaneous gap of our disordered magnet will close as Γ decreases through the quantum phase transition at Γ_c (*20–22*). After that, ground-state level crossings begin. The arrows in Fig. 3 point to two crossings [really avoided crossings (*19*) because the problem possesses no symmetry]. Each instantaneous ground-state crossing is associated with tunneling of the whole system between two valleys, one broad but shallow and the other narrow but deep; such tunneling takes place when kinetic energy diminishes, and represents a major crisis in the otherwise quasi-adiabatic evolution caused by the time-dependent decrease of $\Gamma(t)$.

For sufficiently slow annealing, each tunneling event can be treated as a Landau-Zener (LZ) problem (*23*) (Fig. 3, inset). The probability $P(\tau)$ that the system, starting in the lower state $|b\rangle$ at high Γ, will continue nonadiabatically onto the higher branch as Γ is reduced with time is given by $P(\tau) = \exp(-\tau/\tau_c)$, where the characteristic tunneling time $\tau_c = (\hbar\alpha\Gamma_0)/(2\pi\Delta^2)$, $\hbar$ is Planck's constant divided by 2π, Δ is the tunneling amplitude between the two states $|a\rangle$ and $|b\rangle$ (whose splitting at crossing is 2Δ), and α is the relative slope of the two crossing branches as a function of Γ (*23*). One can estimate $\Delta \approx \exp[-d_{ab}/\xi(\Gamma)]$, where d_{ab} is a suitable distance between states $|a\rangle$ and $|b\rangle$ [in the Ising case, the number of spins flipped in the tunneling process (*21*)], and $\xi(\Gamma)$ is a typical wave function localization length, which must vanish as $\Gamma \to 0$, $\xi(\Gamma) \approx \Gamma^{\psi}$ with some exponent $\psi > 0$. The tunneling time becomes exponentially large for small Γ, $\tau_\Gamma \approx \exp(2d_{ab}/\Gamma^{\psi})$, and an exceedingly small width $\approx \Delta$ of each tunneling event justifies treating the multiple crossings as a cascade of independent LZ events. Once the system fails [with a probability $P_\Gamma(\tau) = \exp(-\tau/\tau_\Gamma)$] to follow the ground state at the LZ crossing occurring at Γ, it will eventually attain an average excitation energy $E_{ex}(\Gamma) > 0$. If we let $Z(\Gamma)d\Gamma$ be the number of LZ crossings taking place between Γ and $(\Gamma + d\Gamma)$, the average residual energy can be estimated as

$$\varepsilon_{res}(\tau) = \int_0^{\Gamma_c} d\Gamma\ Z(\Gamma)\ E_{ex}(\Gamma)\ \exp(-\tau/\tau_\Gamma) \qquad (2)$$

where Γ_c marks the first level crossing. The large τ behavior of this function is dominated by the $\Gamma \to 0$ behavior of $Z(\Gamma)E_{ex}(\Gamma)$, and of τ_Γ. If we assume that, for small Γ, $Z(\Gamma)E_{ex}(\Gamma) \approx \Gamma^{\omega}$ and $\tau_\Gamma \approx \exp(A/\Gamma^{\varphi})$, we finally get $\varepsilon_{res}(\tau) \approx \log^{-\zeta_{QA}}(\tau)$, with an exponent $\zeta_{QA} = (1 + \omega)/\varphi$. The exponents ω and φ are not obvious. A semiclassical expression (*23*) for the decay of a wave function inside a barrier suggests $\varphi = 1/2$. The average excitation energy attained by missing the ground-state "track" at Γ should scale as Γ^2 for small Γ, because all eigenvalues start out as Γ^2 for $\Gamma \to 0$. The total number of LZ crossings occurring from 0 to Γ should not be larger than the number of classical states in the energy window $(E_{GS}, E_{GS} + \Gamma)$, which is approximately equal to $\rho(0)\Gamma$ [where $\rho(0)$ is the density of classical states at the ground state energy (*16*)], so that the density of crossings $Z(\Gamma \to 0) \to \rho(0)$, at most. This yields $\omega = 2$ as our most reasonable estimate.

We conclude that $\zeta_{QA} = (1 + \omega)/\varphi$ can be as large as 6 for a spin glass, and that in any case it is above the classical bound $\zeta \leq 2$ (*3*). Hence, QA of the Ising spin glass is predicted

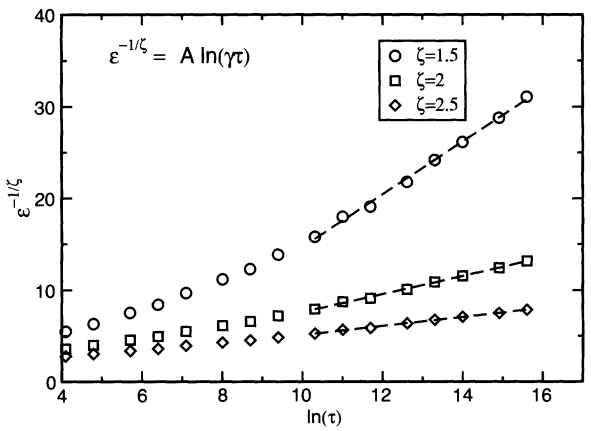

Fig. 2. The same CA data as in Fig. 1, replotted (see text) so as to fall on a straight line if obeying the Huse-Fisher logarithmic law. Although this form is seen to be asymptotically compatible with the data, extraction of a value for the exponent ζ is impossible.

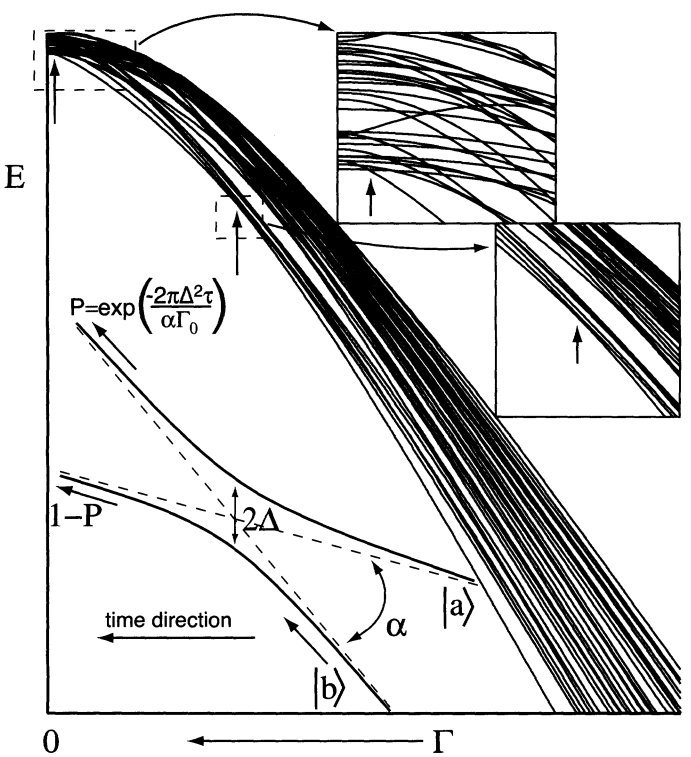

Fig. 3. Cartoon of the lowest instantaneous eigenvalues of a (finite-size) Ising glass as a function of the transverse field Γ, or of a generic complex system as a function of its zero-point kinetic energy Γ. Note the two avoided crossings of the ground state, marked by arrows and enlarged in the upper insets. Lower inset: Schematic of a Landau-Zener crossing. At each crossing the system will follow adiabatically the ground state only if Γ is reduced sufficiently slowly. The infinite system will exhibit an infinite cascade of crossings as $\Gamma \to 0$.

to be again logarithmically accurate, not fundamentally different in this respect from CA. We therefore expect that a quantum computation based on QA will not transform a hard nonpolynomial (NP-complete) computational problem into a polynomial one. On the contrary, the above reasoning suggests that a logarithmically slow annealing also applies to the present 2D Ising case, which is not NP-complete (*14*). The slowing-down effect of the LZ cascade illustrated above is particularly severe in problems, like the Ising spin glass we have considered, where the classical spectrum has a gapless continuum of excitations above the ground state. Satisfiability problems, for which encouraging results were recently presented (*10*), differ from the Ising spin glass in that they possess a discrete classical spectrum and a finite excitation gap. We observe that in general a gap will cut off the LZ cascade precisely in the dangerous low-Γ region, which may eliminate the logarithmic slowing down of QA. Nonetheless, even in the gapless case, the advantage of QA over CA is far from negligible because of the generally larger exponent ζ_{QA} of the logarithm. To get an idea of the order of magnitudes involved, consider the relative increase of annealing time (τ'/τ) needed to improve the accuracy of a certain annealing, say with $\tau \approx 10^6$ (in appropriate units), by a factor of 10. In CA ($\zeta = 2$), this would require $(\tau'/\tau) \approx \tau^{[10^{(1/\zeta)}]-1} \approx 10^{13}$. In QA ($\zeta = 6$), the same result would be accomplished with $(\tau'/\tau) \approx 10^{2.8}$, an enormous saving of computer effort. Moreover, the PIMC version of QA is easy to implement on a parallel computer, which provides an extra advantage. Optimization by QA of a vast variety of problems, after a suitable fictitious kinetic term is identified case by case, is an open avenue and stands as a worthy challenge for the future.

References and Notes

1. S. Kirkpatrick, C. D. Gelatt Jr., M. P. Vecchi, *Science* **220**, 671 (1983).
2. V. Černý, *J. Opt. Theor. Appl.* **45**, 41 (1985).
3. D. A. Huse, D. S. Fisher, *Phys. Rev. Lett.* **57**, 2203 (1986).
4. J. Brooke, D. Bitko, T. F. Rosenbaum, G. Aeppli, *Science* **284**, 779 (1999).
5. J. Brooke, T. F. Rosenbaum, G. Aeppli, *Nature* **413**, 610 (2001).
6. A. B. Finnila, M. A. Gomez, C. Sebenik, C. Stenson, J. D. Doll, *Chem. Phys. Lett.* **219**, 343 (1994).
7. T. Kadowaki, H. Nishimori, *Phys. Rev. E* **58**, 5355 (1998).
8. Y. H. Lee, B. J. Berne, *J. Phys. Chem. A* **104**, 86 (2000).
9. ———, *J. Phys. Chem. A* **105**, 459 (2001).
10. E. Farhi *et al.*, *Science* **292**, 472 (2001).
11. G. S. Grest, C. M. Soukoulis, K. Levin, *Phys. Rev. Lett.* **56**, 1148 (1986).
12. A. Chakrabarti, R. Toral, *Phys. Rev. B* **39**, 542 (1989).
13. P. Ocampo-Alfaro, H. Guo, *Phys. Rev. B* **53**, 1982 (1996).
14. F. Barahona, *J. Phys. A* **15**, 3241 (1982).
15. For each set of couplings, E_{GS} is calculated using the Spin Glass Ground State Server at www.informatik.uni-koeln.de/ls_juenger/projects/sgs.html.
16. D. S. Fisher, D. A. Huse, *Phys. Rev. Lett.* **56**, 1601 (1986).
17. M. Suzuki, *Prog. Theor. Phys.* **56**, 1454 (1976).
18. Supplementary details of the method are available on *Science* Online at www.sciencemag.org/cgi/content/full/295/5564/2427/DC1.
19. E. Lieb, D. Mattis, *J. Math. Phys.* **3**, 749 (1962).
20. H. Rieger, A. P. Young, *Phys. Rev. Lett.* **72**, 4141 (1994).
21. M. J. Thill, D. A. Huse, *Physica A* **214**, 321 (1995).
22. W. Wu, D. Bitko, T. F. Rosenbaum, G. Aeppli, *Phys. Rev. Lett.* **71**, 1919 (1993).
23. L. D. Landau, E. M. Lifshitz, *Quantum Mechanics—Non-Relativistic Theory* (Pergamon, Oxford, 1977).

24. This project was sponsored by the Ministero dell'Istruzione, dell'Università e della Ricerca under project COFIN, by INFM/G, INFM/F, and by INFM's Iniziativa Trasversale Calcolo Parallelo. R.M. acknowledges European Union support through CINECA under project MINOS3, which also provided much of the computer resources. We thank G. Aeppli, L. Arrachea, J. Berg, C. Micheletti, M. Parrinello, F. Ricci Tersenghi, and R. Zecchina for helpful discussions and suggestions.

7 December 2001; accepted 25 February 2002

A Phase Separation Model for the Nanopatterning of Diatom Biosilica

Manfred Sumper*

Diatoms are encased in an intricately patterned wall that consists of amorphous silica. Species-specific fabrication of this ornate biomineral enables taxonomists to identify thousands of diatom species. The molecular mechanisms that control this nanofabrication and generate the diversity of patterns is not well understood. A simple model is described, in which repeated phase separation events during wall biogenesis are assumed to produce self-similar silica patterns in smaller and smaller scales. On the basis of this single assumption, the apparently complex patterns found in the valves of the diatom genus *Coscinodiscus* can be predicted. Microscopic analysis of valves in statu nascendi from three different *Coscinodiscus* species supports the conclusions derived from the model.

Coscinodiscus is regarded as one of the largest genera of marine planktonic diatoms (*1*). The species *Coscinodiscus asteromphalus*, *Coscinodiscus granii*, *Coscinodiscus radiatus*, and *Coscinodiscus wailesii* are frequently found in marine habitats and can be grown in quantities sufficient for biochemical studies (*2*, *3*). Their siliceous cell wall (valve) (Fig. 1A) is a honeycomb consisting of the vertical areolae walls arranged in hexagons (Fig. 1B). Both the roof and the floor of the honeycomb are formed by plates with numerous perforations. The internal plate exhibits a single hole (foramen) exactly in the center of each hexagon. The outside plate is a thin silica layer (cribrum) perforated by a complex but highly symmetric arrangement of pores. The valve structure can be interpreted as a hierarchy of self-similar patterns. Each of the hexagonally arranged chambers (areolae) embodies a set of hexagonally arranged pores (cribrum), and each of these pores in turn embodies a set of even smaller pores in a hexagonal arrangement (cribellum). It is this elaborate patterning that produces the intricate structures observed under the scanning electron microscope (SEM) (Fig. 1C).

The silica shell of diatoms consists of two overlapping valves (Fig. 1A). During cell division, a new valve is formed inside the cell by controlled precipitation of silica within a specialized membrane vesicle called the silica deposition vesicle (SDV) (*4*). Detailed electron microscopic studies by Schmid and Volcani (*5*) led to a phenomenological description of wall morphogenesis in *C. wailesii*. According to this work, definite stages of silica deposition within the SDV can be discerned during morphogenesis of a new valve. Initially, development of the base layer containing the foraminae is followed by the construction of the hexagonally arranged walls of the areolae. The outer layer (cribrum and cribellum) are completed later. A particular feature of outer-layer construction is that fabrication of the cribrum is centripetal in relation to the areolae, that is, fabrication of the cribrum on top of each areola begins at the hexagonally arranged walls and continues toward the middle of each areola. Finally, all the pores within a cribrum are further modified by precipitating silica to establish the cribellum.

A mechanistic model of wall morphogenesis should explain not only the creation of particular patterns but also the growth behavior of cribra and cribella. An earlier model for pattern formation based on electron microscopic observations postulated a complex and highly regulated assembly of different cell organelles and vesicles creating a precisely shaped mold for the expanding SDV and the precipitating silica in it (*6*). However, the cellular mechanism that could control the

Lehrstuhl Biochemie I, Universität Regensburg, 93053 Regensburg, Germany.

*E-mail: manfred.sumper@vkl.uni-regensburg.de